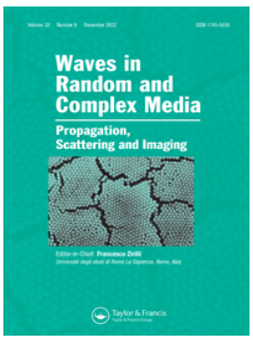

Waves in Random and Complex Media

ISSN: (Print) (Online) Journal homepage: https://www.tandfonline.com/loi/twrm20

Convected heat and mass transport in magnetic burgers' nanoliquid subject to chemical responses

Kotha Gangadhar, M. Prameela, K. Venkata Ramana & Ali J. Chamkha

To cite this article: Kotha Gangadhar, M. Prameela, K. Venkata Ramana & Ali J. Chamkha (2022): Convected heat and mass transport in magnetic burgers' nanoliquid subject to chemical responses, Waves in Random and Complex Media, DOI: 10.1080/17455030.2022.2118396

To link to this article: https://doi.org/10.1080/17455030.2022.2118396

Published online: 14 Sep 2022.

WAVES IN RANDOM AND COMPLEX MEDIA
https://doi.org/10.1080/17455030.2022.2118396

Convected heat and mass transport in magnetic burgers' nanoliquid subject to chemical responses

Kotha Gangadhar[a], M. Prameela[b], K. Venkata Ramana [c] and Ali J. Chamkha[d]

[a]Department of Mathematics, AcharyaNagarjuna University Campus, Ongole, India; [b]Department of Mathematics, Prasad V. Potluri Siddharth Institute of Technology, Kanuru, India; [c]Department of Mathematics, Vardhana College of Engineering, Hyderabad, India; [d]Faculty of Engineering, Kuwait College of Science and Technology, Doha, Kuwait

ABSTRACT

This paper investigates the effect of Burgers' nanofluid convinced as a stretching cylinder on heat source about magnetohydrodynamic stagnation point flow. Effect of the heat source/sink and chemical reaction are more appropriate to consider mass and heat transportation to the flow of Burgers' fluid. Additionally, the effects of different convective actions i.e. convective condition by the exterior subordinate as two mass and heat transport arejoined in the analysis. The mathematical formulation was collected as the absorbing boundary layer theory and later coincidence transformations were imported in governing partial differential equations. The solutions of velocity, solutal, and thermal equations were declined to results, and graphs are interpreted from practical judgments. Fundamental physical announcement to the flow figure by Burgers' nanofluid improvement the lowering ideals magnetic force parameter. Also, The flow pattern of Burgers fluid parameters is contrary to the fluid detention time parameter. Furthermore, it was derived the thermal sketch and thermal density to the boundary layer of nanofluid enhance values of thermal Biot number and heat source parameter. The current examination was guaranteed to be recognised as study with previously presented scheduled.

ARTICLE HISTORY
Received 24 March 2022
Accepted 23 August 2022

KEYWORDS
Burgers fluid; nanofluid; heat rise/fall; multiple convective conditions; stagnation point flow

Nomenclature

(u_1, w_1)	Velocity components (ms^{-1})
(r_1, z_1)	Cylindrical coordinates (m)
j_m	Mass flux
q_m	Heat flux
ν	Kinematic viscosity (m^2s^{-1})
C_1	Fluid concentration
C_f	Concentration at the surface
C_∞	Ambient concentration
T_1	Fluid temperature (K)

CONTACT Ali J. Chamkha a.chamkha@kcst.edu.kw

T_f	The temperature at the surface (K)
T_∞	Ambient temperature (K)
Le	Lewis number
Nb	Brownian motion parameter
A	Velocity ratio parameter
Bi_1	Thermal Biot number
Bi_2	Mass Biot number
M	Magnetic parameter
Pr	Prandtl number
k_1	Chemical reaction rate
Nt	Thermophoresis parameter
c_f	Specific heat ($Jkg^{-1}K^{-1}$)
w_e	Free stream velocity (ms^{-1})
w_s	Stretching velocity (ms^{-1})
k	Thermal conductivity ($Wm^{-1}K^{-1}$)
h_f	Convective heat transport coefficient ($Wm^{-2}K^{-1}$)
h_m	Convective mass transport coefficient (ms^{-1})
R	Radius of the cylinder (m)
D_B	Brownian diffusion coefficient (m^2s^{-1})
D_T	Thermophoretic coefficient (m^2s^{-1})

Greek symbols

ρ_f	Density ($kg\,m^{-3}$)
β_1	Fluid relaxation parameter
β_2	Burgers fluid parameter
β_3	Fluid retardation parameter
α_1	Thermal diffusivity (m^2s^{-1})
α	Curvature parameter
δ	Heat source/sink parameter
$\tilde{\theta}$	Dimensionless temperature
$\tilde{\phi}$	Dimensionless concentration
λ_1	Fluid relaxation time
λ_2	The material parameter of the Burgers fluid
λ_3	Fluid retardation time

1. Introduction

The cooling, heating, and engineering are done as they are essential to raise the performance of the thermodynamic system. Hence, the extended demand from different heat exchanges was current. In any case, a limited to existing heat transaction had to be earned previously. Thus, advanced fluids from competent heat transfer are improved. Other fluids are nanofluids. The nanofluid was a mix of nanometer-sized (1–100 nm) particles and the base fluid. Every nanoparticle is joined to commonly metal oxide or metal. The thermal conductivity coefficients of metals are greater than those of traditional fluids [1]. Ekiciler [2] studied the heat transfer and flow features of the two-dimensional conduit bottom-forced

transmission. Tibaut et al. [3] focused on the course inspecting for laminar mixed convection of nanofluid that the pipe. Their outcome displays the temperature field to the fluid and in the pipe, built upon actively for the nanoparticle concentration circulation. Shehzad et al. [4] performed an analytical study on convective mass and heat conditions to the boundary layer flow of nanofluid. Acharya [5] conducted the thermal radiated nanofluidic to bring completely bent exterior, with more functions employing nanofluid [6–17]. Commonly, heat transfer in nanofluids is greater than the conventional fluids as well as oil, ethylene glycol, water, etc.

Mostly, the Burgers fluid was the non-Newtonian fluid. The non-Newtonian texture had a compelling consequence and enough physical function time that engineers and researchers scrutinized in the study. Better to recycle evidence to the biochemical, geophysical, and petrochemical move on non-Newtonian basis. This evidence has been restricted to integral, differential, and rate from materials. Investigators collected impressive debate on rate-type categories and differential in a sketch. The Burgers fluid profile was studied by the viscoelastic rate-type fluid sketch that was largely matured profile. The Burgers model showed the foundation of stress relaxation on many polymeric fluids. Hayat et al. [18] described that boundary layer flow on the Burgers nanofluid a way the existence of Robin's form condition by the stretching exterior bottom condition for the applied magnetic field. Khan et al. [19] described the nonlinear thermal radiation of the flow by the Burgers fluid convinced as a stretching cylinder under the consideration for chemical reaction. Abel et al. [20] suggested that the flow of upper-convected Maxwell fluid be investigated for heat transport. Waqas et al. [21] presented a detailed experiment about the mixed convection flow of Oldroyd-B nanoliquid under thermal and solutal stratifications. The consequence of chemical reactions for the flow of Oldroyd-B fluid on the stretched cylinder was considered by Irfan et al. [22]. Khan et al. [23] investigated the existence of Cattaneo-Christov heat flux theory as Burgers fluid features completed stretching cylinder. Nagaraja and Gireesha [24] demonstrated a numerical investigation for Casson fluid flow completed curved stretching sheet in addition to convective heat and mass flux, chemical reaction, and boundary conditions.

Fluid mechanics for the analysis of the stagnation point flow had an extreme consequences and real-world functions in industry, such as flows identified completed edge to blowing of fiberglass and jets and submarines and the spinning, etc. Similar constructive function investigators showed more consideration to stagnation point flows and examined flows theoretically. Nguyen et al. [25] consider mixed convection flow of nanofluid adjacent is vertical wall as investigation from basics to passive and active control. The three-dimensional stagnation point flow over a wavy cylindrical shaped body was carried out by Riaz et al. [26]. The hybrid nanofluid flow of the non-axisymmetric stagnation point field to the flat plate on the porous medium was investigated by Waini et al. [27]. Xie and Wang [28] described stagnation point flow and heat transfer of the power law fluid path over the stretching exterior along the heat generation effect. Even unsteady boundary layer stagnation point flow and heat transfer of fractional Maxwell fluid due to the power-law-dependent stretching plate under the influence of generalized Fourier's law theory was analyzed by Bai et al. [29]. Shafiq et al. [30] conducted a theoretical investigation for double stratification features on Walter's B nanoliquid consumed over the Riga surface.

Every circumstance on an orderly heat sink/source had recognizable applications as medicine and more engineering actions related to cooling to metallic sheets, every intention to substance behavior, unfinished oil cure, etc. Usman et al. [31] presented a heat transfer circumstance about power–law fluid along a non-uniform heat source/sink inside flexible disks. Acharya and Mabood [32] conducted a numerical study for hydrothermal features in the pair of hybrid nanofluid and usual nanofluid flow by the perilous passable limp formation. The characteristics of rectangular convective flow on nanoliquid by the extend plate exact from partial slip were discussed by Mahanthesh et al. [33]. Tufail et al. [34] inspected the two-dimensional MHD boundary layer flow on the higher-convected Maxwell fluid fleeting over the shrinking sheet to thermal radiation. Roy and Pop [35] reported both results via mixed convection flow by the Oldroyd-B fluid complete alumina nanoparticles converted by the magnetic field effect. Further associating modules could be established in Refs. [36–55].

Burgers' fluid was the non-Newtonian fluid that has more applications for industries and engineering, such as petrochemical, geophysical and biochemical applications. Included in that unit are benefits for exploring every appearance of mass transfer as engaging influence on chemical reactions to the stagnation point flow of magnetised Burgers' nanofluid acquired at stretching cylinder. Convective mass and heat transport conditions are utilized by heat growth/fall influence. Mathematical modeling to flow phenomenon was developed for the PDE and popularized correlation transformations were followed for ODEs. The numerical programme bvp4c method was used to inspect the physical behaviour of ramified flow, solutal distributions, and temperature parameters. Every numerical value for coefficients to heat and mass transfer rates by Burgers nanoliquid was depicted as computed in the table.

2. Mathematical formulation

The current issue is the exchange from steady 2D incompressible flow of Burgers' nanofluid. Furthermore, the researchers examine that the flow was considered for the stretching cylinder with radius R nearby stagnation point. Give cylindrical polar coordinates (r_1, z_1) from such as surround to z_1-axis with axis to the cylinder and r_1-axis with radial guidance by concluded over (Figure 1). Velocity field as current flow was studied by $= [u_1, 0, w_1]$. Here, u_1 and w_1 are taken by the velocity entrails with r_1 and z_1 axis, appropriately. Flow equation to Burgers' nanofluid beyond the stretching cylinder was modeled and integrated among orderly magnetic field $B = [B_0, 0, 0]$ enforced perpendicular for the flow guidance. Also, every energy equation was modeled and integrated by the characteristics of the heat source/sink, while chemical reactions and nanoparticles are again considered with the figure for the concentration equation. Additionally, it's accepted such the cylinder was stretched with the z_1-direction by velocity $w_s = \frac{U_0 z_1}{l}$; here U_0 was studied to allusion velocity and l was the exact length. As well, physically many real convective mass and heat transport conditions are integrated by the boundary of the exterior. The plate was heated as transmission to the boiling fluid from the temperature $T_f(> T_\infty)$ contributes to the heat transfer coefficient h_f. Finally, the thermal convective boundary condition develops. Furthermore, the absorption of the plate $C_f(> C_\infty)$ contributes to the mass transfer coefficient h_m.

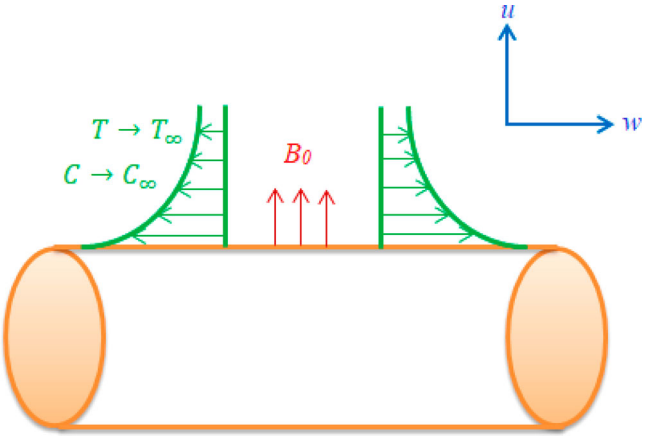

Figure 1. Flow configuration.

Established from the above assumption, the essential noted equations based on the applicable system are defined in refs. [18, 23]:

$$\frac{\partial u_1}{\partial r_1}+\frac{u_1}{r_1}+\frac{\partial w_1}{\partial z_1}=0, \tag{1}$$

$$\begin{aligned}
&u_1\frac{\partial w_1}{\partial r_1}+w_1\frac{\partial w_1}{\partial z_1}+\lambda_1\left[u_1^2\frac{\partial^2 w_1}{\partial r_1^2}+w_1^2\frac{\partial^2 w_1}{\partial z_1^2}+2u_1w_1\frac{\partial^2 w_1}{\partial z_1\partial r_1}\right]\\
&+\lambda_2\left[\begin{array}{l}
u_1^3\frac{\partial^3 w_1}{\partial r_1^3}+w_1^3\frac{\partial^3 w_1}{\partial z_1^3}+2u_1^2\left(\frac{\partial u_1}{\partial r_1}\frac{\partial^2 w_1}{\partial r_1^2}+\frac{\partial w_1}{\partial r_1}\frac{\partial^2 w_1}{\partial r_1\partial z_1}\right)\\
-u_1^2\left(\frac{\partial w_1}{\partial r_1}\frac{\partial^2 u_1}{\partial r_1^2}+\frac{\partial w_1}{\partial z_1}\frac{\partial^2 w_1}{\partial r_1^2}\right)\\
+2w_1^2\frac{\partial u_1}{\partial z_1}\frac{\partial^2 w_1}{\partial r_1\partial z_1}+w_1^2\left(\frac{\partial w_1}{\partial z_1}\frac{\partial^2 w_1}{\partial z_1^2}-\frac{\partial w_1}{\partial r_1}\frac{\partial^2 u_1}{\partial z_1^2}\right)\\
+3u_1w_1\left(u_1\frac{\partial^3 w_1}{\partial r_1^2\partial z_1}+w_1\frac{\partial^3 w_1}{\partial z_1^2\partial r_1}\right)\\
+2u_1w_1\left(\frac{\partial u_1}{\partial r_1}\frac{\partial^2 w_1}{\partial z_1\partial r_1}+\frac{\partial u_1}{\partial z_1}\frac{\partial^2 w_1}{\partial r_1^2}+\frac{\partial w_1}{\partial r_1}\frac{\partial^2 w_1}{\partial z_1^2}-\frac{\partial w_1}{\partial r_1}\frac{\partial^2 u_1}{\partial r_1\partial z_1}\right)
\end{array}\right]\\
&=w_e\frac{\partial w_e}{\partial r_1}+\upsilon\lambda_3\left[\begin{array}{l}
u_1\frac{\partial^3 w_1}{\partial r_1^3}+w_1\frac{\partial^3 w_1}{\partial r_1^2\partial z_1}+\frac{u_1}{r_1}\frac{\partial^2 w_1}{\partial r_1^2}-\frac{\partial w_1}{\partial r_1}\frac{\partial^2 u_1}{\partial r_1^2}\\
+\frac{w_1}{r_1}\frac{\partial^2 w_1}{\partial r_1\partial z_1}-\frac{1}{r_1}\frac{\partial u_1}{\partial r_1}\frac{\partial w_1}{\partial r_1}-\frac{1}{r_1}\frac{\partial w_1}{\partial r_1}\frac{\partial w_1}{\partial z_1}-\frac{\partial w_1}{\partial z_1}\frac{\partial^2 u_1}{\partial r_1^2}
\end{array}\right]\\
&+\upsilon\left[\frac{\partial^2 w_1}{\partial r_1^2}+\frac{1}{r_1}\frac{\partial w_1}{\partial r_1}\right]-\frac{\sigma B_0^2}{\rho}\left[(w_1-w_e)+\lambda_1u_1\frac{\partial w_1}{\partial r_1}\right.\\
&\left.+\lambda_2\left(w_1\frac{\partial u_1}{\partial z_1}\frac{\partial^2 w_1}{\partial r_1^2}-u_1\frac{\partial w_1}{\partial z_1}\frac{\partial^2 w_1}{\partial r_1^2}+u_1w_1\frac{\partial^2 w_1}{\partial r_1\partial z_1}+u_1^2\frac{\partial^2 w_1}{\partial r_1^2}\right)\right],
\end{aligned} \tag{2}$$

$$u_1\frac{\partial T_1}{\partial r_1}+w_1\frac{\partial T_1}{\partial z_1}=\alpha_1\frac{1}{r_1}\left[\frac{\partial}{\partial r_1}\left(r_1\frac{\partial T_1}{\partial r_1}\right)\right]+\tau\left[D_B\frac{\partial C_1}{\partial r_1}\frac{\partial T_1}{\partial r_1}+\frac{D_T}{T_\infty}\left(\frac{\partial T_1}{\partial r_1}\right)^2\right]+\frac{Q_0(T_1-T_\infty)}{(\rho c)_f}, \tag{3}$$

$$u_1\frac{\partial C_1}{\partial r_1}+w_1\frac{\partial C_1}{\partial z_1}=\frac{D_B}{r_1}\frac{\partial}{\partial r_1}\left(r_1\frac{\partial C_1}{\partial r_1}\right)+\frac{D_T}{T_\infty}\frac{1}{r_1}\frac{\partial}{\partial r_1}\left(r_1\frac{\partial T_1}{\partial r_1}\right)-k_0(C_1-C_\infty), \tag{4}$$

with boundary conditions

$$w_1=w_s=\frac{U_0z_1}{l},u_1=0,-k_f\frac{\partial T_1}{\partial r_1}=h_f(T_f-T_1),-D_m\frac{\partial C_1}{\partial r_1}=h_m(C_f-C_1)\,\text{at}\,r_1=R, \tag{5}$$

$$w_1\to w_e=\frac{U_\infty z_1}{l},\ \frac{\partial w_1}{\partial r_1}\to 0,\ T_1\to T_\infty,\ C_1\to C_\infty,\ \text{as}\,r_1\to\infty. \tag{6}$$

Here, (u_1,w_1) are the components of velocity in r_1 and z_1 indication, υ is the kinematics viscosity, (C_1,T_1) are the liquid concentration and temperature, respectively, Q_0 is the heat generation/absorption coefficient, w_s is the stretching velocity, $\alpha_1=\left(\frac{k}{(\rho c)_f}\right)$ is the thermal diffusivity, in which (ρ_f,c_f) is the density of the liquid and specific heat.

They now introduce the below dimensionless functions ensuing [23] into converting fundamental equation via a non-dimensionless model:

$$\begin{aligned}&u_1=-\frac{R}{r_1}\sqrt{\frac{U_0\upsilon}{l}}\tilde{g}(\tilde{\eta}),\ w_1=\frac{U_0z_1}{l}\tilde{g}'(\tilde{\eta}),\ \tilde{\eta}=\sqrt{\frac{U_0}{\upsilon l}}\left(\frac{r_1^2-R^2}{2R}\right),\\&\tilde{\theta}(\tilde{\eta})=\frac{T_1-T_\infty}{T_f-T_\infty},\ \tilde{\phi}(\tilde{\eta})=\frac{C_1-C_\infty}{C_f-C_\infty}.\end{aligned} \tag{7}$$

Later substituting the above modifications Equation (1) was convinced naturally and Equation's (2)–(5) output.

$$\begin{aligned}&(1+2\alpha\tilde{\eta})^2\beta_1[2\tilde{g}\,\tilde{g'}\,\tilde{g''}-\tilde{g}^2\tilde{g'''}]-(1+2\alpha\tilde{\eta})\alpha\beta_1\tilde{g}^2\tilde{g''}\\&-(1+2\alpha\tilde{\eta})^2\beta_2[3\tilde{g}^2\,\tilde{g''}^2+2\tilde{g}\,\tilde{g'}^2\,\tilde{g''}-\tilde{g}^3\tilde{g}^{iv}]-4\alpha^2\beta_2\tilde{g'''}\,\tilde{g''}\\&+(1+2\alpha\tilde{\eta})\alpha\beta_2[3\tilde{g}^2\tilde{g'}\,\tilde{g''}+\tilde{g}^3\,\tilde{g'''}]+(1+2\alpha\tilde{\eta})^3\beta_3[\tilde{g''}^2-\tilde{g}\,\tilde{g}^{iv}]\\&-4\alpha\beta_3(1+2\alpha\tilde{\eta})^2\tilde{g}\,\tilde{g'''}+(1+2\alpha\tilde{\eta})^3\tilde{g'''}+(1+2\alpha\tilde{\eta})^2[2\alpha\tilde{g''}+\tilde{g}\,\tilde{g''}-\tilde{g'}^2]\\&+(1+2\alpha\tilde{\eta})^2A^2-(1+2\alpha\tilde{\eta})^2M^2[\beta_2\tilde{g}\,\tilde{g'''}-\beta_1\tilde{g}\,\tilde{g''}+\tilde{g'}-A]=0,\end{aligned} \tag{8}$$

$$(1+2\alpha\tilde{\eta})\tilde{\theta''}+2\alpha\tilde{\theta'}+\text{Pr}\,\tilde{g}\tilde{\theta'}+\text{Pr}\,Nb\,\tilde{\theta'}\,\tilde{\phi'}(1+2\alpha\tilde{\eta})+\text{Pr}\,Nt\,\tilde{\theta'}^2(1+2\alpha\tilde{\eta})+\text{Pr}\,\delta\tilde{\theta}=0, \tag{9}$$

$$(1+2\alpha\tilde{\eta})\,\tilde{\phi''}+2\alpha\,\tilde{\phi'}+Le\,\text{Pr}\,\tilde{g}\tilde{\phi'}+(1+2\alpha\tilde{\eta})\left(\frac{Nt}{Nb}\right)\tilde{\theta''}+2\alpha\left(\frac{Nt}{Nb}\right)\tilde{\theta'}-\text{Pr}\,Le\,k_1\tilde{\phi}=0, \tag{10}$$

Modified boundary conditions are as follows:

$$\tilde{g}=0,\tilde{g'}=1,\ \tilde{\theta'}+Bi_1(1-\tilde{\theta})=0,\ \tilde{\phi'}+Bi_2(1-\tilde{\phi})=0,\ \text{at}\,\tilde{\eta}=0, \tag{11}$$

$$\tilde{g'}\to A,\ \tilde{g''}\to 0,\ \tilde{\theta}\to 0,\ \tilde{\phi}\to 0,\ \text{as}\,\tilde{\eta}\to 0. \tag{12}$$

Dimensionless parameters are defined as follows:

$$A=\frac{U_\infty}{U_0},\ \alpha=\frac{1}{R}\sqrt{\frac{\upsilon l}{U_0}},\ \beta_1=\lambda_1\frac{U_0}{l},\ \beta_3=\lambda_3\frac{U_0}{l},\ \beta_2=\lambda_2\left(\frac{U_0}{l}\right)^2,\ M=\left(\frac{\sigma lB_0^2}{\rho_f U_0}\right)^{1/2},$$
$$Le=\frac{\alpha_1}{D_B},\ \mathrm{Pr}=\frac{\upsilon}{\alpha_1},\ k_1=\frac{k_0 l}{U_0},\ \delta=\frac{lQ_0}{U_0(\rho c)_f},Nt=\frac{\tau D_T(T_f-T_\infty)}{\upsilon T_\infty},$$
$$Bi_1=\frac{h_f}{k_f}\sqrt{\frac{\upsilon l}{U_0}},\ Nb=\frac{\tau D_B(C_f-C_\infty)}{\upsilon},Bi_2=\frac{h_m}{D_m}\sqrt{\frac{\upsilon l}{U_0}}. \tag{13}$$

Physical concern parameters:

The rate of mass transport (Sh_z) and its relations to the rate of heat transfer (Nu_z) are

$$Nu_z=\frac{z_1 q_m}{k(T_f-T_\infty)},\ Sh_z=\frac{z_1 j_w}{D_B(C_f-C_\infty)}. \tag{14}$$

Here j_m and q_m were the mass and heat flux, respectively

$$q_m=-k\left(\frac{\partial T_1}{\partial r_1}\right)_{r_1=R},\ j_m=-D_B\left(\frac{\partial C_1}{\partial r_1}\right)_{r_1=R}. \tag{15}$$

This dimensionless model Equation (14) is yielded by

$$\begin{aligned} Nu_z Re^{-1/2}&=-\theta'(0),\\ Sh_z Re^{-1/2}&=-\phi'(0), \end{aligned} \tag{16}$$

where $Re_z=\frac{w(z_1)z_1}{\upsilon}$ is the local Reynolds number.

3. Numerical procedure

The present section grants the numerical explanation form as dimensionless nonlinear temperature, momentum, and concentration equations. Equations (8)–(10) for the boundary conditions Equations (11) and (12) are resolved numerically by having the bvp4c technique and the particular collection method that needs the Lobatto-III-A formula. By confining to that method, every system of higher-order partial differential equations was converted into first-order ordinary differential equations by recommending a few modern variables [46–47]:

$$g=\tilde{\Psi}_1,\ g'=\tilde{\Psi}_2,\ g''=\tilde{\Psi}_3,\ g'''=\tilde{\Psi}_4,\ \theta=\tilde{\Psi}_5,\ \theta'=\tilde{\Psi}_6,\ \phi=\tilde{\Psi}_7,\ \phi'=\tilde{\Psi}_8 \tag{17}$$

$$\tilde{\Psi}_4'=\frac{1}{\left[\begin{array}{l}(1+2\alpha\tilde{\eta})^3\tilde{\Psi}_1\beta_3\\ -(1+2\alpha\tilde{\eta})^2\beta_2\tilde{\Psi}_1^3\end{array}\right]}\left[\begin{array}{l}(1+2\alpha\tilde{\eta})^2\beta_1[2\tilde{\Psi}_1\,\tilde{\Psi}_2\,\tilde{\Psi}_3-\tilde{\Psi}_1^2\tilde{\Psi}_4]\\ -(1+2\alpha\tilde{\eta})\alpha\beta_1\tilde{\Psi}_1^2\tilde{\Psi}_3+(1+2\alpha\tilde{\eta})^3\tilde{\Psi}_4\\ -4\alpha^2\beta_2\tilde{\Psi}_4\,\tilde{\Psi}_3-4\alpha\beta_3(1+2\alpha\tilde{\eta})^2\tilde{\Psi}_1\,\tilde{\Psi}_4\\ -(1+2\alpha\tilde{\eta})^2\beta_2[3\tilde{\Psi}_1^2\,\tilde{\Psi}_3^2+2\tilde{\Psi}_1\,\tilde{\Psi}_2^2\,\tilde{\Psi}_3]\\ +(1+2\alpha\tilde{\eta})\alpha\beta_2[3\tilde{\Psi}_1^2\tilde{\Psi}_2\,\tilde{\Psi}_3+\tilde{\Psi}_1^3\,\tilde{\Psi}_4]\\ +(1+2\alpha\tilde{\eta})^2[2\alpha\,\tilde{\Psi}_3+\tilde{\Psi}_1\,\tilde{\Psi}_3-\tilde{\Psi}_2^2]\\ +(1+2\alpha\tilde{\eta})^3\beta_3[\tilde{\Psi}_3^2]\\ -(1+2\alpha\tilde{\eta})^2M^2\left[\begin{array}{l}\beta_2\tilde{\Psi}_1\,\tilde{\Psi}_4-\beta_1\tilde{\Psi}_1\,\tilde{\Psi}_3\\ +\tilde{\Psi}_2-A\end{array}\right]\\ +(1+2\alpha\tilde{\eta})^2A^2=0,\end{array}\right], \tag{18}$$

Table 1. The observation table as $-f''(0)$ opposed to various values of β_1 at $\alpha = \beta_3 = M = \beta_2 = 0$.

β_1	Abel et al. [20]	Waqas et al. [21]	Irfan et al. [22]	Khan et al. [23]	Present outcomes
0.0	1.000000	1.000000	1.0000000	1.0000000	1.00000000
0.2	1.051948	1.051889	1.0518890	1.0518891	1.05188987
0.4	1.101850	1.101903	1.1019035	1.1019036	1.10190326
0.6	1.101850	1.150137	1.1501374	1.1501375	1.15013734
0.8	1.196692	1.196711	1.1967114	1.1967015	1.19671126
1.0	–	–	1.2417477	1.2417699	1.24174748
1.2	1.285257	1.285363	1.2853630	1.2853701	1.28536327
1.4	–	–	1.3276675	1.3276669	1.32762478
1.6	10368641	1.368758	1.3687582	1.3687579	1.36876929
1.8	–	–	1.4087264	1.4087310	1.40874630
2.0	1.447617	1.447651	1.4476526	1.4476519	1.44765066

Table 2. Parallel investigation of current outcomes as $-f''(0)$ opposed to various values of M when $\alpha = \beta_3 = \beta_1 = \beta_2 = 0$.

M	Shehzad et al. [4]	Hayat et al. [18]	Khan et al. [19]	Current outcomes
0.0	1.00000	1.00000	1.000000	1.0000000
0.2	1.01980	1.01980	1.019801	1.0198039
0.5	1.11803	1.11803	1.118029	1.1180340
0.8	1.28063	1.28063	1.280633	1.2806248
1.0	1.41421	1.41421	1.414221	1.4142136
1.2	1.56205	1.56205	1.562048	1.5620499
1.5	1.80303	1.80303	1.803044	1.8027756

$$\tilde{\Psi}_6' = -\frac{1}{(1+2\alpha\tilde{\eta})}\left[\begin{array}{l} 2\alpha\ \tilde{\Psi}_6 + \mathrm{Pr}\,\tilde{\Psi}_1\tilde{\Psi}_6 + (1+2\alpha\tilde{\eta})\,\mathrm{Pr}\,Nb\tilde{\Psi}_6\tilde{\Psi}_8 \\ +\mathrm{Pr}\,Nt(1+2\alpha\tilde{\eta})\tilde{\Psi}_6^2 + \mathrm{Pr}\,\delta\ \tilde{\Psi}_5 \end{array}\right], \tag{19}$$

$$\Psi_8{}' = -\frac{1}{(1+2\alpha\tilde{\eta})}\left[\begin{array}{l} 2\alpha\ \tilde{\Psi}_8 + Le\,\mathrm{Pr}\,\tilde{\Psi}_1\tilde{\Psi}_8 + (1+2\alpha\tilde{\eta})\left(\frac{Nt}{Nb}\right)\tilde{\Psi}'_6 \\ +2\alpha\left(\frac{Nt}{Nb}\right)\ \tilde{\Psi}_6 - Le\,\mathrm{Pr}\,k_1\tilde{\Psi}_7 \end{array}\right], \tag{20}$$

with

$$\Psi_1(0) = 0.\ \Psi_2(0) = 1,\ \Psi_6(0) + Bi_1(1 - \Psi_5(0)) = 0,\ \Psi_8(0) + Bi_2(1 - \Psi_7(0)) = 0, \tag{21}$$

$$\Psi_2(\infty) = A,\ \Psi_3(\infty) = 0,\ \Psi_5(\infty) = 0,\ \Psi_7(\infty) = 0. \tag{22}$$

4. Validation of results

In this study, the numerical computations are presented for the validation of local skin friction, as shown in Tables 1 and 2. This comparison with Refs [20–23] shows the effects of the Deborah number β_1 on local skin friction by keeping other parameters zero; this is presented in Table 1. Similarly, Table 2 shows the correlation between $-\tilde{g}''(0)$ during related magnitudes M along with a few earlier presented modules [4, 18, 19]. Thus, they could declare that our effort was accurate by comparing with the already presented outcomes.

5. Results and discussion

The area for the unit are conversing to natural explanation by physical parameters and that is convoluted in this nonlinear differential Equations (8)-(10) made up of approximate boundary conditions specified at Equations (11) and (12). They selected the bvp4c

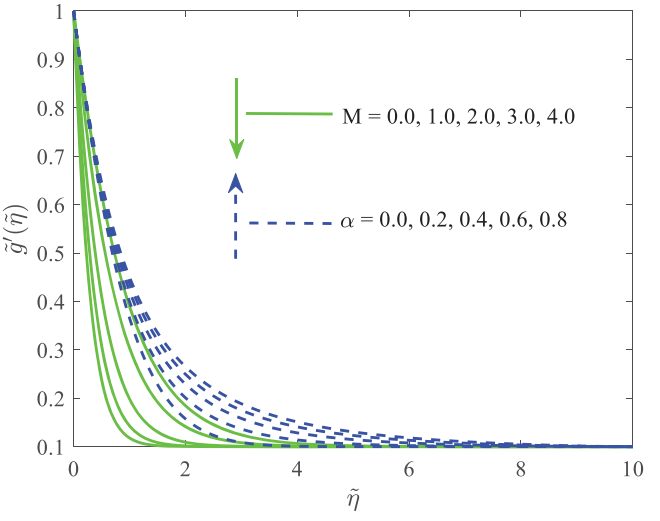

Figure 2. Influence of M and α as the flow sketch.

method examining to influence physical parameters in flow, thermal, and concentration transportation by the Burgers fluid. This influence on total fundamental physical parameters was noted and determined along the entire physical kindly and then affected results are seen in Figures 2–15. They inspected the effects of stagnation parameter (A), heat source/sink (δ), Brownian motion factor (Nb), the constraints of curvature (α), fluid relaxation time (β_1), the material factor of the Burgers fluid (β_2), fluid retardation time (β_3) and thermal $\tilde{\theta}(\tilde{\eta})$ and concentration $\tilde{\phi}(\tilde{\eta})$ distributions of Burgers fluid, the magnetic force (M) on flow $\tilde{g}'(\tilde{\eta})$, although the influence of Prandtl number (Pr), thermophoresis factor (Nt) shows thermal curves and the influence of the Lewis number (Le) and the chemical reaction parameter (k_1) is noticed as solutal curves by the Burgers magneto fluid. The solutions performed in the current investigation have the parameters in the range $M \in [0.0, 4.0], \alpha \in [0.0, 0.8], \beta_1 \in [0.0, 3.2], \beta_2 \in [0.1, 0.5], \beta_3 \in [2.5, 6.5], A \in [1.5, 3.5], \delta \in [-0.4, 0.4], Pr \in [0.71, 5.0], Bi_1 \in [0.7, 1.5], Le \in [1.0, 10.0], Nt \in [0.1, 0.5], Nb \in [0.3, 1.1], Bi_2 \in [0.7, 1.5], k_1 \in [-0.5, 0.5]$ with fixed $Pr = 6.2, \beta_1 = 0.7, \beta_2 = 0.25, \beta_3 = 0.5, A = 0.1, M = 0.2, Le = 1.0, \delta = 0.2, Bi_1 = 1.8, Bi_2 = 1.8$ and $k_1 = 0.5$.

In Equations (8–12), if $\lambda_1 = \lambda_2 = \lambda_3$ and $\lambda_1 = \lambda_3$ are the couple essentials that effort decreases on Newtonian model, $\lambda_2 = 0$ as model decrease on Oldroyd B fluid model, and $\lambda_2 = \lambda_3 = 0$ as model decrease on Maxwell fluid model. Here $k_1 = 0$ indicates the non-chemical reactive Burgers fluid. $\delta = 0$ describes the absence of a heat source/sink. $M = 0$ indicates the hydrodynamic flow situation and $M \neq 0$ shows the hydromagnetic flow of the Burgers fluid.

They are describing the physical indication by total convoluted parameters along the acceptable explanation. Figure 2 shows the physical analysis by the magnetic factor and curvature parameter for velocity profiles of the Burgers fluid. This delayed to the flow curves on the fluid into greater being more curvature parameter is shown in the figure. Every moderation on the radius by the cylinder shrinks over the adjustment of curvature and the outcome cooperation field on fluid along the calculation again is defined. Thus, deduction was formed on the protection as long as surface and basically the fluid velocity and the

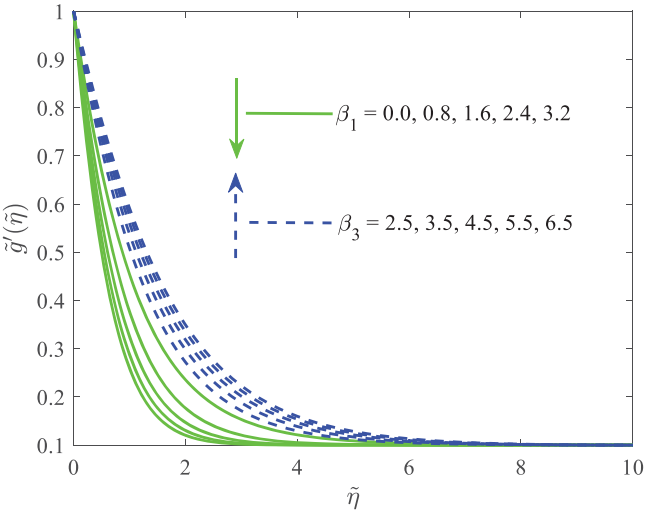

Figure 3. Influence of β_1 and β_3 as the flow sketch.

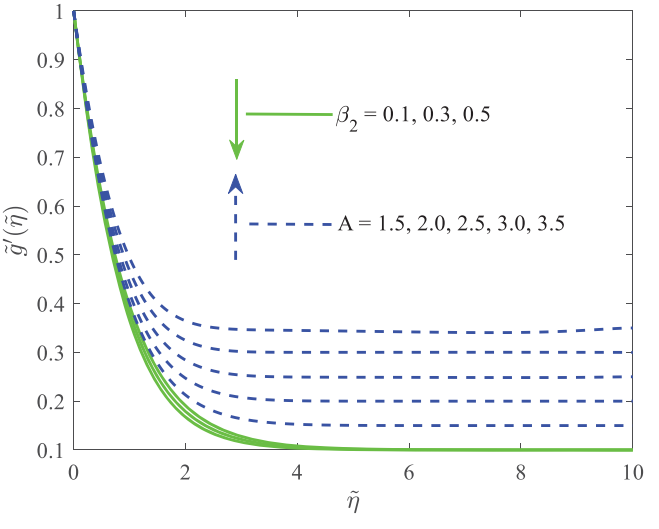

Figure 4. Influence of β_2 and A as the flow sketch.

identical density on boundary layer expansion. Furthermore, this figure, which is complete to the momentum boundary layer converts skinny and velocity sketched to Burgers nanoliquid dwindle as an enhancement to the values of magnetic field factor. Physically, in every augmentation for a magnetic parameter, the resistive force, termed Lorentz force, was composed. That force hampers velocity of the liquid inside of the boundary layer field when the motion of the liquid shows a decline. That, velocity distribution to nanoliquid downturn for enhancement as M.

The effects of relaxation time and retardation time parameters against flow profiles of nano Burgers fluid are shown in Figure 3. It shows that the flow sketch and approximate boundary layer thickness by the Burgers nanofluid decrease the increment of β_1, because

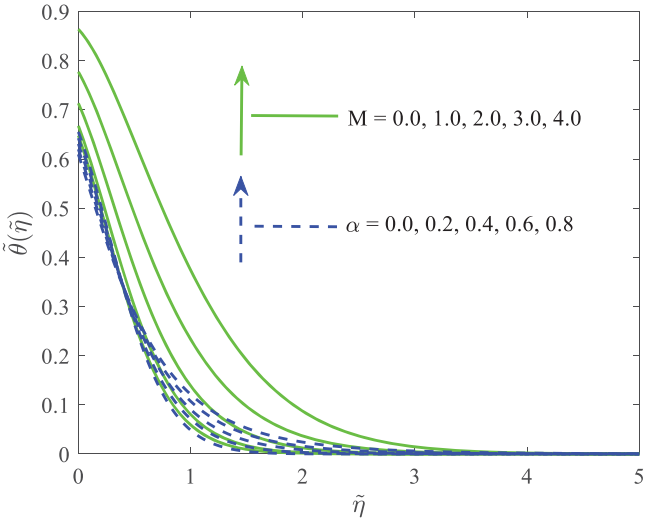

Figure 5. Influence of M and α on the thermal figure.

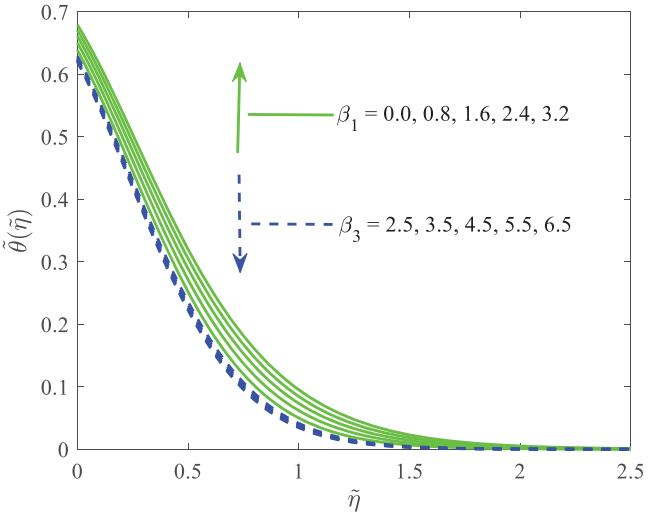

Figure 6. Influence of β_1 and β_3 on the thermal figure.

it increases with an increment β_3. Physically, β_1 this was the ratio to relief for consideration degree. Hence, relief time complement to enhancement that Deborah's number, and, therefore, intransigence for fluid motion raises to the point as dwindle for velocity sketch. Furthermore, β_3 calculates retardation time λ_3. Thus, the enhancement the retardation time β_3 too improved. Therefore, stimulation was composed of fluid flow and fluid velocity improvement.

Figure 4 depicts the characteristics of the Burgers fluid parameter and the velocity ratio parameter with respect to the Burgers nanofluid. It was exposed to flow phenomena and the identical density to the boundary layer of Burgers liquid raises to the acceleration on the magnitude of velocity ratio constant ($A < 1$) for those plots. Basically, $A = \frac{w_e}{w_s}$ as the ratio of

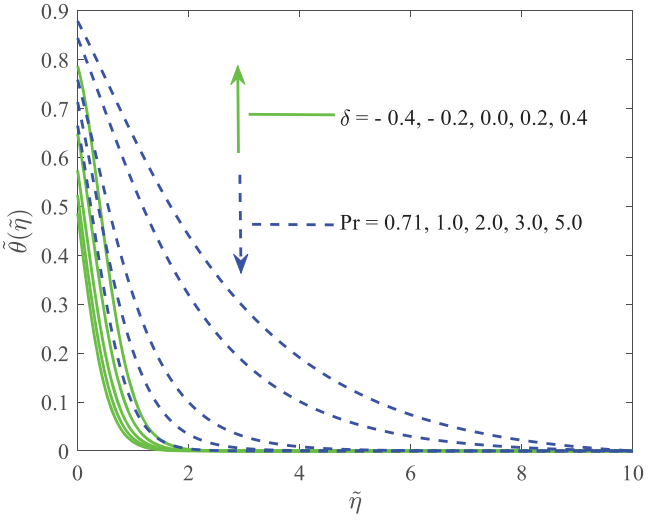

Figure 7. Influence of δ and *Pr* as the thermal sketch.

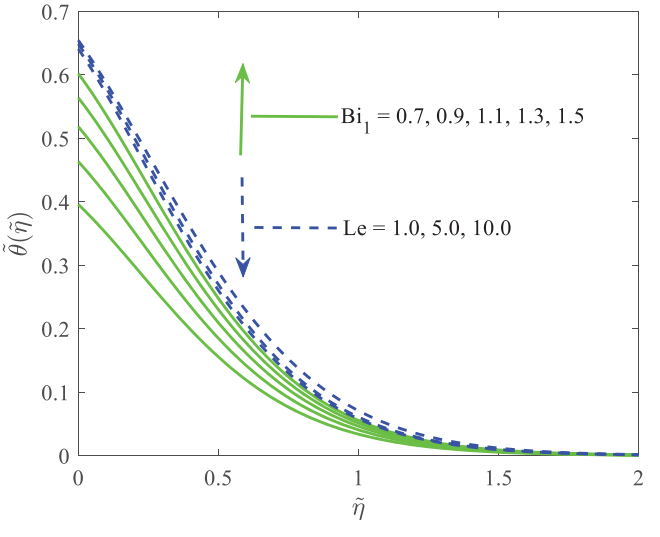

Figure 8. Influence of Bi_1 and *Le* on the thermal sketch.

free stream velocity is (w_e) about the stretching velocity on the cylinder (w_s). Because, the condition $(A < 1)$ harmonizes that the position to interpret for velocity the free stream was insignificant to relate the velocity for the stretching cylinder. Naturally, as the magnitude of A increases, the velocity of the free stream increases, and the fluid flows at a high speed. As the $A = 1$ boundary layer would not be perfect, it was necessary to position the velocity about the free stream equivalent to the velocity of the stretching cylinder, which complicated the fluid motion and boundary motion to equal rates. Moreover, from this profile, it can be observed to the flow figure as the Burgers fluid becomes uncertain by aggravating for the magnitude of the Burgers fluid parameter. Literally, as the Burgers fluid parameter

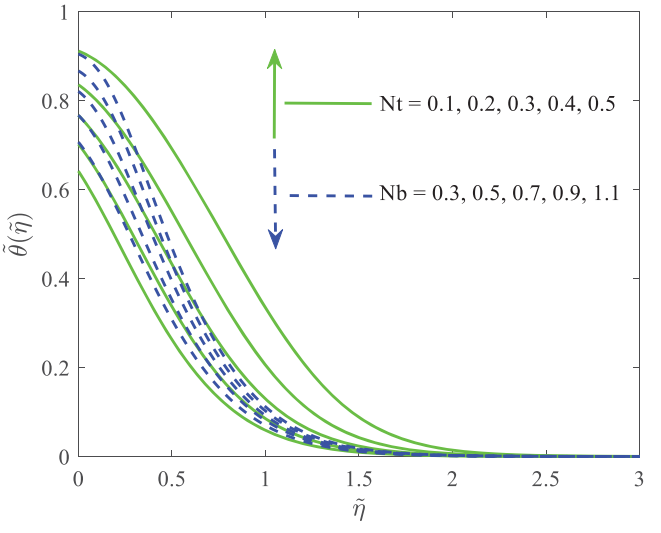

Figure 9. Influence of *Nt* and *Nb* as the thermal sketch.

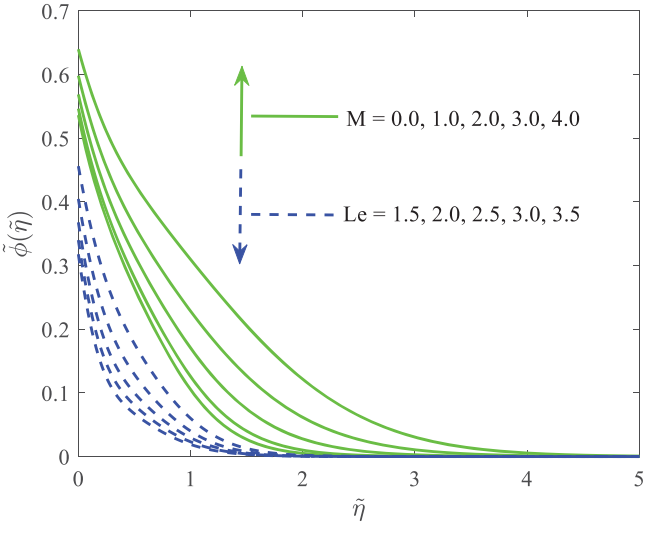

Figure 10. Influence of *M* and *Le* as the solutal sketch.

increases, the factor stress relaxation time (λ_2) intensifies time to that fluid influence the act as solid type and, as a result, the flow figure deteriorates.

Figure 5 shows that the temperature distribution of the Burgers fluid accelerates for an enhancement in both the strengthening of the magnetic field and curvature parameter. Physically, the increasing Lorentz force devise as well as communication among the fluid particles time to that higher extant for heat was arising to the system and accordingly thermal figure to nano liquid complement and identical thickness of boundary layer convert broad. As well as, it's assumed the the greater values of α improvement couple the thermal

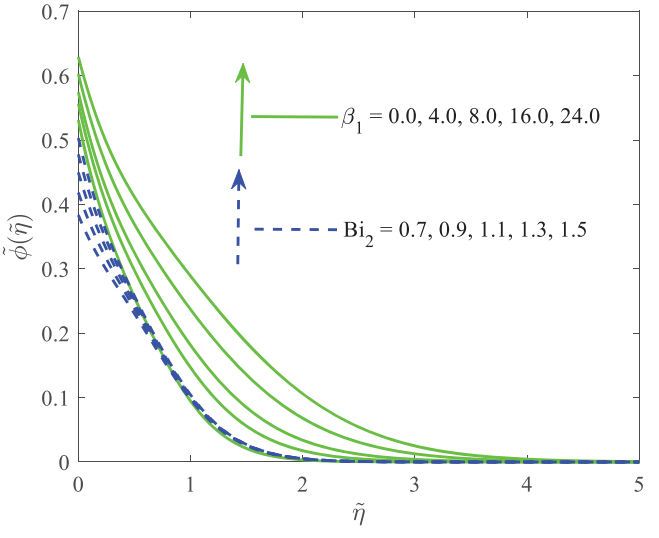

Figure 11. Influence of β_1 and Bi_2 as the solutal sketch.

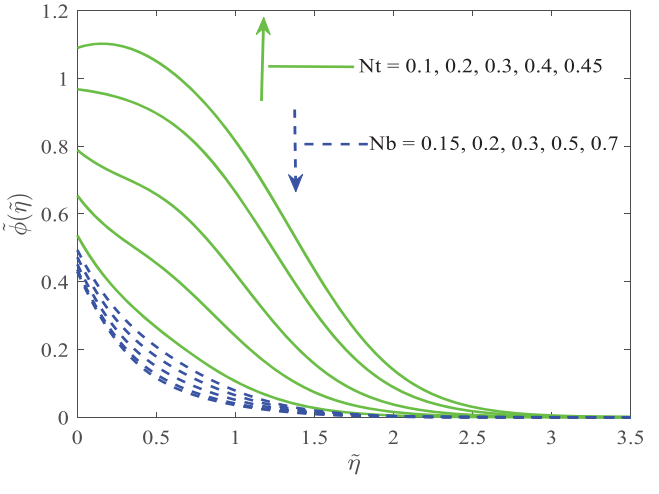

Figure 12. Influence of *Nt* and *Nb* as the solutal sketch.

sketch and identical thickness of the boundary layer. It is now up to the intellect to extant for heat transport increases that result in boosting the thermal profiles of Burgers nano liquid.

Figure 6 analyzes the influence on leisure and retardation due to parameters against thermal profile. When β_1 complements, the leisure due to more complemented time for communication among fluid particles raises; therefore, the thermal profile of the Burgers nanofluid enhances. Furthermore, retardation due to complement along amplification to Deborah number that was important to reduce direction to thermal sketch and identical Burgers nanoliquid boundary layer thickness. Furthermore, it is noticed about time the existence of relaxation and retardation because they noticed that temperature had altogether contra effects for β_1 as compared to β_3.

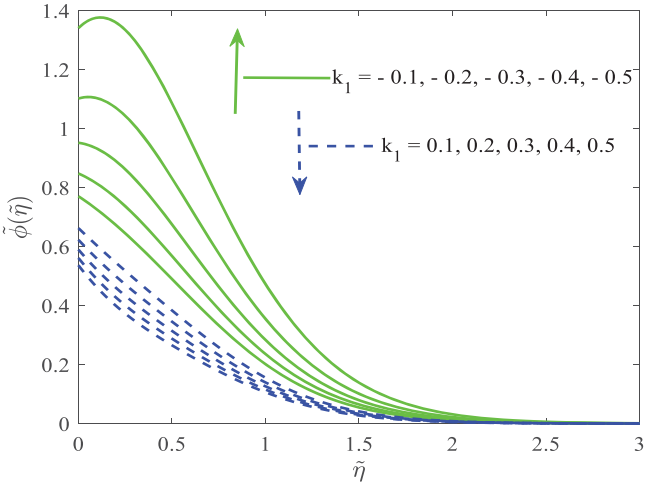

Figure 13. Influence of k_1 as the solutal sketch.

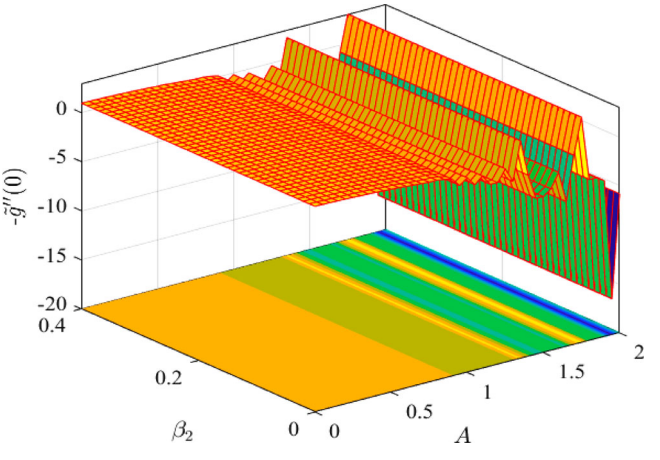

Figure 14. Influence of β_2 and A as skin friction.

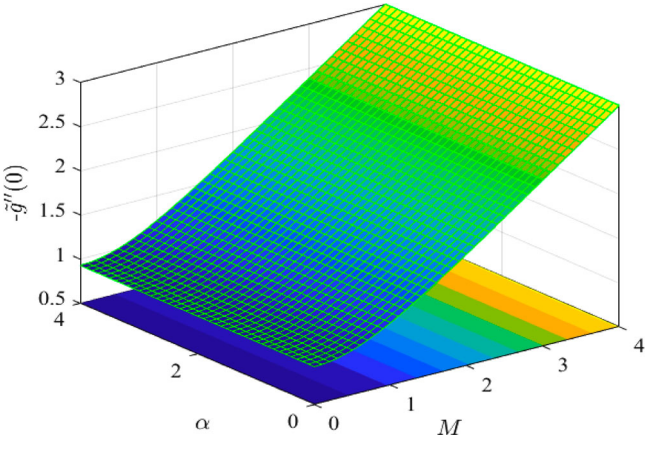

Figure 15. Influence of α and M as skin friction.

Figure 7 acknowledges the temperature component to the effects of heat source/sink constraints and Prandtl number. The thermal curves on Burgers liquid illustrate ascending direction to heat source parameter ($\delta > 0$) when illustrating the descending action of heat sink constraint ($\delta < 0$). It was easy, i.e. the effect of several sources of heat was expended to the system when the thermal circulation for the fluid escalates, and the comparison away from, they are expanding the values of heat sink constraint their large measure of heat impact on allowance the system when certain temperature to the system decreases. Furthermore, weakening to the thermal profile of nano Burgers liquid is presumed, then values of the Prandtl number increase. Away from hand, the thermal boundary layer thickness like incline delicate to more *Pr*, when the case from *Pr* bet on thermal diffusivity than come to anaemic thermal diffusivity outcomes on decrease to the temperature figure and like the thermal boundary layer thickness decreases.

Figure 8 depicts the components of the thermal Biot number and Lewis number as they relate to the temperature profile. Furthermore, it was revealed that the temperature distribution and the identical thickness by boundary layer of Burgers fluid decrease with an increase in the Lewis number. Additionally, as Bi_1 raises, transfers to heat over transmission appear mostly. Therefore, acceleration to thermal curves could be seen. A similar pattern was noticed by Nagaraja and Gireesha [24].

The impacts of Brownian motion and thermophoresis parameters against temperature distribution are shown in Figure 9. It shows the thermal figure of nanoliquid frame up and the thermal thickness of the boundary layer develops the largest number of *Nt*. Naturally, thermophoresis illustrates from evolution that insignificant particles form as temperature gradients. So, thermophoresis concession in deportation to also heated particles over the surface by the temperature gradient. Additionally, temperature rose the growing Brownian parameter. Literally, it is about increasing the Brownian motion parameter to augment the random motion of insignificant nanoparticles. Although the haphazard movement of metallic particles boost, frictional collision among the fragments was established. Hence the hatched frictional heat is going to cool the thermal sketch. An equal outcome was observed by Acharya [5].

The focal point to effects of magnetic parameter and Lewis number contra concentration circulation as the Burgers nanofluid, as shown in Figure 10. Concentration and solutal boundary layer thickness were recorded in developing values as *M*. Also, the Lewis number was the ratio of momentum diffusivity and mass diffusivity and was backword comparable to the mass diffusion coefficient. As a result of the search for the Lewis number margin for decline from diffusion, the result was a decrease in the mass of nanoparticles solutal boundary layer and volume fraction.

Figure 11 depicts the effects of the relaxation time factor and Biot number (Bi_2) on the absorption figure of the Burgers nanofluid. It was a common fact although relaxation time raises, fluid concentration and associated thickness of the boundary layer boost. Thus, the concentration sketch raises with β_1. Another point is that the concentration Biot number grows, mass diffusivity downturns and so, fluid concentration raises. Hence, at Bi_2 raises, concentration field embellishment is shown in Figure 11. Such consequences are supported by Nagaraja and Gireesha [24].

The graph of concentration curves of nano Burgers fluid to Brownian motion and the exaggerated values of thermophoresis are shown in Figure 12. The nanoparticle volume fraction of Burgers liquid enhances along with *Nt*. Hence, solute boundary layers

Table 3. Impact on physical parameters on heat and mass transfer rates.

β_2	Pr	Nt	Q	Bi_1	Bi_2	Nb	$-\theta'(0)$	$-\phi'(0)$
0.0	6.2	0.2	0.2	1.8	1.8	0.2	0.440927	0.849728
0.1							0.438708	0.848276
0.2							0.436412	0.846775
0.3							0.434037	0.845226
0.4							0.431579	0.843625
S_{lp}							**−0.000018573**	**−0.000007916**
0.25	0.71						0.197725	0.347429
	1.0						0.250440	0.407219
	2.0						0.372271	0.561444
	3.0						0.422712	0.662054
	5.0						0.445685	0.792653
	S_{lp}						**0.012543183**	**0.04632795**
	6.2	0.1					0.540534	0.949978
		0.2					0.435235	0.846007
		0.3					0.323156	0.719478
		0.4					0.197858	0.540375
		0.5					0.015764	0.235999
			S_{lp}				**−0.058408241**	**−0.110285769**
		0.2	−0.4				0.748103	1.132294
			−0.2				0.695994	1.083714
			0.0				0.632144	1.024365
			0.2				0.550036	0.948855
			0.4				0.435235	0.846007
			S_{lp}				**−0.021005994**	**−0.017574691**
				0.5			0.299080	0.936377
				1.0			0.390459	0.883498
				1.5			0.424416	0.856415
				2.0			0.440447	0.840531
				2.5			0.449391	0.830215
				S_{lp}			**0.005249599**	**−0.002511635**
				1.8	0.5		0.518644	0.332314
					1.0		0.479266	0.573568
					1.5		0.449668	0.756293
					2.0		0.426697	0.899302
					2.5		0.408395	1.014182
					S_{lp}		**−0.002610705**	**0.099788105**
					1.8	0.1	0.522157	0.621716
						0.2	0.435235	0.846007
						0.3	0.351585	0.918576
						0.4	0.273071	0.953185
						0.5	0.201261	0.972666
						S_{lp}	**−0.02193134**	**0.028888701**

and momentum develop raising values of Nt. Furthermore, Brownian motion authorities from diffusion to the nanoparticles establish further the boundary. Thus, augmentation from Brownian motion parameter outcomes reduces nanoparticles' volume fraction sketch.

Figure 13 determines the influence of chemical reaction parameters (k_1^+, k_1^-) opposed to concentration circulation based on the Burgers nanoliquid as the couple negative and positive values. This graph contained such nanoparticles' volume fraction reduction and the approximate boundary layer became more delicate during the rising values of k_1^+. This comparison is noticed to solutal form about the Burgers nanoliquid frame up and density based on the boundary layer upgrade along inflation in values of k_1^-. This capable chemical reaction parameter (k_1^+) correlates in avoiding this mass transfer and upgrading as larger values as k_1^-.

The variation in dimensionless skin friction $-\tilde{g}''(0)$ against distinct values about the velocity ratio parameter (A) and the Burgers fluid parameter (β_2) are shown in Figure 14. It shows that drag skin friction coefficient boosts with a rise in β_2 at the rate 0.096158 while it deceases at the rate -3.50951 with an increment in A. Figure 15 shows the influence of the curvature factor (α) and magnetic parameter (M) against the drag skin friction coefficient by a boundary. This was observed to supply skin friction by the exterior hike at the rate 0.554784 for the higher magnitude of M while it decreases at the rate -0.01286 for higher values of α.

Table 3 highlights the variations of $\beta_2, Pr, Nt, \delta, Bi_1, Bi_2$ and Nb for dimensionless Nusselt and Sherwood numbers. The straight relapse slop at Table 3 depicts this Pr and Bi_1 yield the rate of heat transport raise by the rate 0.012543183 and 0.005249599, while $\beta_2, Nt, \delta, Bi_2$ and Nb show the rate of heat transfer decrement at the rates -0.000018573, -0.058408241, -0.021005994, -0.002610705 and -0.021931343, respectively. Overflow study by Table 3 determines the enlargement of mass transfer rate by that rates 0.04632795, 0.099788105 and 0.028888701 for incremental values of Pr, Bi_2 and Nb while it was decreased by at the rates -0.000007916, -0.110285769, -0.017574691 and -0.002511635 for β_2, Nt, δ, and Bi_1, respectively. Table 2 is about $-\tilde{g}''(0)$ as district values by M for a few modules. The effect, against that table, they have ensured this the new results are appropriately detailed.

6. Concluding remarks

The analytical analysis being stagnation point flow convinced over the stretched cylinder by magnetic nano Burgers' fluid on the combination for heat source/sink and chemical reaction impacts have been made. Additionally, multiple convective mass and heat conditions are integrated into this study. A numerical procedure, namely the bvp4c method, had been appropriated in the report based on outcomes. A luminary result of our determination is given as follows:

1. The motion of every Burgers' fluid shows by increasing the magnitude of the magnetic force parameter and relaxation time factor, although the acceleration was decreased by raising the curvature factor and the rate of velocity ratio parameter.
2. The flow arrangement based on Burgers' fluid parameter performs contrary to a fluid detention time parameter.
3. Prandtl and Lewis' numbers are advantaged through the deterioration of the transportation of thermal thickness and thermal energy away from the boundary layer inside the flow.
4. Temperature dissemination about the Burgers liquid appreciates as a heat source parameter $(\delta > 0)$ although the reversal behavior was observed during heat sink constraint$(\delta < 0)$.
5. The solutal thickness and concentration rate about the boundary layer by a Burgers fluid hike up as changeable the degree about magnetic force parameter and fluid relaxation time factor.
6. The deficiency of solutal thickness away from the boundary layer was noticed as positive expanding values about chemical reaction parameters (k_1^+) although reversal direction was exhibited as being negatively expanding values (k_1^-).

7. Drag skin friction decreases for increasing curvature factor and stagnation parameter against the magnetic force factor.
8. The mass and heat moving are decreased for Burgers' fluid parameter and thermophoresis parameter against the Prandtl number.

The present investigation concluded the potential implication of Burgers' nanofluid through a non-porous stretching cylinder. Further studies will focus on exploring the porous stretching cylinder with transient effects.

Disclosure statement

No potential conflict of interest was reported by the author(s).

ORCID

K. Venkata Ramana http://orcid.org/0000-0002-1316-3824

References

[1] He W, Toghraie D, Lotfpour A, et al. Effect of twisted-tape inserts and nanofluid on fow feld and heat transfer characteristics in a tube. Int Commun Heat Mass Transf. 2020;110:104440.
[2] Ekiciler R. Effects of novel hybrid nanofluid (TiO2-Cu/EG) and geometrical parameters of triangular rib mounted in a duct on heat transfer and flow characteristics. J Therm Anal Calorim. 2021;143:1371–1387.
[3] Tibaut J, Tibaut T, Ravnik J. Numerical solution of mixed convection of a nanofluid in a circular pipe with different numerical models. J Therm Anal Calorim. 2021;145:2525–2534.
[4] Shehzad SA, Hayat T, Alsaedi A. Influence of convective heat and mass conditions in MHD flow of nanofluid. Bull Pol Acad Sci Tech Sci. 2015;63(2):465–474.
[5] Acharya N. Spectral quasi linearization simulation of radiative nanofluidic transport over a bended surface considering the effects of multiple convective conditions. Eur J Mech/B Fluids. 2020;84:139–154.
[6] Zhao C, An W, Zhang Y, et al. Impact of enhances electric field on light-induced evaporation process of plasmonic nanofluid. Int J Heat Mass Transf. 2022;189:122708.
[7] Dong J, Zheng Q, Xiong C, et al. Experimental investigation and application of stability and thermal characteristics of SiO2-ehtylene-glycol/water nanofluids. Int J Therm Sci. 2022;176:107533.
[8] Hojjat M. Numerical simulation and multi-objective optimization of heat transfer of Al2O3/water nanofluid in rectangular ducts. Int J Therm Sci. 2022;172:107343.
[9] Surendran VS, Bindhu B, Indulal CR, et al. Highly stable ZrO2/silicone oil nanofluid for cutting fluid application. Arab J Sci Eng. 2022;47:949–956.
[10] Rao MVS, Gangadhar K, Chamkha AJ, et al. Bioconvection in a convectional nanofluid flow containing gyrotactic microorganisms over an isothermal vertical cone embedded in a porous surface with chemical reactive species. Arab J Sci Eng. 2021;46:2493–2503.
[11] Gireesha BJ, Gangadhar K, Sindhu S. Entropy generation analysis of electrical magnetohydrodynamic flow of TiO2-Cu/H2O hybrid nanofluid with partial slip. Int J Numer Method H. 2021;31(6):1905–1929.
[12] Venkata Ramana K, Gangadhar K, Kannan T, et al. Cattaneo-Christove heat flux theory on transverse MHD Oldroyd-B liquid over nonlinear stretched flow. J Therm Anal Calorim. 2022;147:2749–2759.
[13] Gangadhar K, Seshakumari PM, Venkata Subba Rao M, et al. MHD flow analysis of a Williamson nanofluid due to Thomson and Troian slip condition. Int A Appl Comput Math. 2022;8:6.
[14] Lei J, Luo Z, Qing S, et al. Effect of surfactants on the stability, rheological properties, and thermal conductivity of Fe3O4 nanofluids. Powder Technol. 2022;399:117197.

[15] Kazemian A, Khatibi M, Maadi SR, et al. Performance optimization of a nanofluid-based photovoltaic thermal system integrated with nano-enhanced phase change material. Appl Energy. 2021;295:116859.
[16] Mehdi M, Afshin H, Morteza M, et al. Mixed convection in a ventilated enclosure by considering both geometrical parameters and thermo-physical properties of water/Cu nanofluid. J Therm Sci. 2021;30:950–961.
[17] Hamid M, Seyed Mostafa TG, Alimorad R, et al. A novel approach for energy and water conservation by using silver-carbon quantum dots hybrid nanofluids in wet cooling towers system. J Therm Sci. 2021;30:1827–1841.
[18] Hayat T, Waqas M, Shehzad SA, et al. On model of Burgers fluid subject to magneto nanoparticles and convective conditions. J Mol Liq. 2016;222:181–187.
[19] Khan M, Iqbal Z, Ahmed A. Stagnation point flow of magnetized Burgers' nanofuid subject to thermal radiation. Appl Nanosci. 2020;10:5233–5246.
[20] Abel MS, Tawade JV, Nandeppanavar MM. MHD flow and heat transfer for the upper-convected Maxwell fluid over a stretching sheet. Meccanica. 2012;47:385–393.
[21] Waqas M, Khan MI, Hayat T, et al. Stratified flow of an Oldroyd-B nanoliquid with heat generation. Results Phys. 2017;7:2489–2496.
[22] Irfan M, Khan M, Khan WA. Impact of homogeneous-heterogeneous reactions and non-Fourier heat flux theory in Oldroyd-B fluid with variable conductivity. J Braz Soc Mech Sci Eng. 2019;41:135.
[23] Khan M, Iqbal Z, Ahmed A. A mathematical model to examine the heat transport features in Burgers fluid flow due to stretching cylinder. J Therm Anal Calorim. 2022;147:827–841.
[24] Nagaraja B, Gireesha BJ. Exponential space-dependent heat generation impact on MHD convective flow of Casson fluid over a curved stretching sheet with chemical reaction. J Therm Anal Calorim. 2021;143:4071–4079.
[25] Nguyen MN, Sajjad T, Le TH, et al. Modified Chebyshev wavelets approach for mixed convection flow due to oblique stagnation point along a vertically moving surface with zero mass flux of nanoparticles. J Mol Liq. 2021;343:117569.
[26] Riaz N, Qasim M, Afridi MI, et al. Analysis of three-dimensional stagnation point flow over a radiative surface. Int Commun Heat Mass Transf. 2021;127:105538.
[27] Waini I, Ishak A, Pop I. Symmetrical solutions of hybrid nanofluid stagnation-point flow in a porous medium. Int Commun Heat Mass Transf. 2022;130:105804.
[28] Xie B, Wang YM. Stagnation-point flow and heat transfer of power-law MHD fluid over a stretching surface with convective heat transfer boundary condition. Int J Numer Method H. 2022;32(1):265–282.
[29] Bai Y, Huo L, Zhang Y. Unsteady stagnation-point flow and heat transfer of fractional Maxwell fluid towards a time dependent stretching plate with generalized Fourier's law. Int J Numer Method H. 2021;31(4):1345–1368.
[30] Shafiq A, Mebarek-Oudina F, Sindu TN, et al. A study of dual stratification on stagnation point Walters' B nanofluid flow via radiative Riga plate: a statistical approach. Eur Phys J Plus. 2021;136:407.
[31] Usman, Lin P, Ghaffari A. Steady flow and heat transfer of th power-law fluid between two stretchable rotating disks with non-uniform heat source/sink. J Therm Anal Calorim. 2021;146:1735–1749.
[32] Acharya N, Mabood F. On the hydrothermal features of radiative Fe3O4-graphene hybrid nanofluid flow over a slippery bended surface with heat source/sink. J Therm Anal Calorim. 2021;143:1273–1289.
[33] Mahanthesh B, Thriveni K, Lorenzini G. Significance of nonlinear Boussinesq approximation and non-uniform heat source/sink on nanoliquid flow with convective heat condition: sensitivity analysis. Eur Phys J Plus. 2021;136:418.
[34] Tufail MN, Saleem M, Chaudhry QA. An analysis of Maxwell fluid through a shrinking sheet with thermal slip effect: a Lie group approach. Indian J Phys. 2021;95:725–731.
[35] Roy NC, Pop I. Dual solutions of magnetohydrodynamic mixed convection flow of an Oldroyd-B nanofluid over a shrinking sheet with heat source/sink. Alex Eng J. 2022;61(8):5939–5948.

[36] Li YX, Israr U, Rehman M, et al. Dynamics of Casson nanoparticles with non-uniform heat source/sink: A numerical analysis. Ain Shams Eng J. 2022;13(1):101496.
[37] Agrawal P, Dadheech PK, Jat RN, et al. Radiative MHD hybrid-nanofluids flow over a permeable stretching surface with heat source/sink embedded in porous medium. Int J Numer Method H. 2021;31(8):2818–2840.
[38] Ramesh GK, Madhukesh JK. Activation energy process in hybrid CNTD and induced magnetic slip flow with heat source/sink. Chin J Phys. 2021;73:375–390.
[39] Akram J, Akbar NS, Maraj E. Chemical reaction and heat source/sink on magnetonano Prandtl-Eyring fluid peristaltic propulsion in an inclined symmetric channel. Chin J Phys. 2020;65:300–313.
[40] Afshar SR, Mishra SR, Sattar Dogonchi A, et al. Dissection of entropy production for the free convection of NEPCMs-filled porous wavy enclosure subjected to volumetric heat source/sink. J Taiwan Inst Chem Eng. 2021;128:98–113.
[41] Selimefendigil F, Akbulut Y, Sengur A, et al. MHD conjugate natural convection in a porous cavity involving a curved conductive partition and estimations by using long short-term memory networks. J Therm Anal Calorim. 2020;140:1457–1468.
[42] Mahabaleshwar US, Rekha MB, Vinay Kumar PN, et al. Mass transfer characteristics of MHD Casson fluid flow past stretching/shrinking sheet. J Engin Thermophys. 2020;29:285–302.
[43] Selimefendigil F, Oztop HF. Impacts of using an elastic fin on the phase change process under magnetic field during hybrid nanoliquid convection through a PCM-packed bed system. Int J Mech Sci. 2022;216:106958.
[44] Selimefendigil F, Oztop HF. Role of magnetic field and surface corrugation on natural convection in a nanofluid filled 3D trapezoidal cavity. Int Commun Heat Mass Transf. 2018;95:182–196.
[45] Chamkha AJ, Selimefendigil F. MHD free convection and entropy generation in a corrugated cavity filled with a porous medium saturated with nanofluids. Entropy. 2018;20(11):846.
[46] Ahmed J, Shahzad A, Farooq A, et al. Thermal analysis in swirling flow of titanium dioxide-aluminum oxide water hybrid nanofluid over a rotating cylinder. J Therm Anal Calorim. 2021;144:2175–2185.
[47] Ahmed A, Khan M, Ahmed J. Thermal analysis in swirl motion of Maxwell nanofluid over a rotating circular cylinder. Appl Math Mech-Engl Ed. 2020;41:1417–1430.
[48] Hafeez A, Khan M, Ahmed J. Oldroyd-B fluid flow over a rotating disk subject to Soret-Dufour effects and thermophoresis particle deposition. Proc Inst Mech Eng C J Mech Eng Sci. 2021;235(13):2408–2415.
[49] Khan M, Ahmed J, Sultana F, et al. Non-axisymmetric Homann MHD stagnation point flow of Al_2O_3-Cu/water hybrid nanofluid with shape factor impact. Appl Math Mech-Engl Ed. 2020;41:1125–1138.
[50] Ahmed J, Khan M, Ahmad L. Radiative heat flux effect in flow of Maxwell nanofluid over a spiraling disk with chemically reaction. Phys A: Stat Mech Appl. 2020;551:123948.
[51] Ahmed A, Khan M, Ahmed J, et al. Mixed convection in unsteady stagnation point flow of Maxwell fluid subject to modified Fourier's law. Arab J Sci Eng. 2020;45(11):9439–9447.
[52] Ahmed J, Shahzad A, Farooq A, et al. Radiative heat transfer in Homann stagnation-point flow of hybrid nanofluid. Appl Nanosci. 2020;10:5305–5314.
[53] Khan M, Ahmed J, Ahmad L. Chemically reactive and radiative von Karman swirling flow due to a rotating disk. Appl Math Mech-Engl Ed. 2018;39:1295–1310.
[54] Hafeez A, Khan M, Ahmed A, et al. Rotational flow of Oldroyd-B nanofluid subject to Cattaneo-Christov double diffusion theory. Appl Math Mech-Engl Ed. 2020;41:1083–1094.
[55] Khan M, Ahmed A, Ahmed J. Boundary layer flow of Maxwell fluid due to torsional motion of cylinder: modeling and simulation. Appl Math Mech-Engl Ed. 2020;41:667–680.